

Modelling of evaporation from free water surface

Wei-Kang Song* and Yibo Chen^a

School of Civil Engineering, Zhengzhou University, 100 Science Avenue, Zhengzhou, China

(Received June 18, 2019, Revised March 11, 2020, Accepted March 16, 2020)

Abstract. The process of evaporation from free water surface was simulated in a large scale environmental chamber under various controlled atmospheric conditions and also was modelled by a new mass transfer model. Six evaporation tests were conducted with increasing wind speed and air temperature in the environmental chamber, and hence the effect of atmosphere parameters on the evaporation process and the corresponding response of water were investigated. Furthermore, based on the experiment results, seven general types of mass transfer models were evaluated firstly, and then a new model consisted of wind speed function and air relative humidity function was proposed and validated. The results show that the free water evaporation is mainly affected by the atmospheric parameters and the evaporation rate increases with the increasing air temperature and wind speed. Both the air and soil temperatures are affected by the energy transformation during water evaporation. The new model can satisfactorily describe the evaporation process from free water surface under different atmospheric conditions.

Keywords: free water surface; evaporation rate; mass transfer model; environmental chamber

1. Introduction

Water evaporation from free water surface (e.g., pools, lakes, rivers, reservoirs, etc.) is a critical water cycle in the nature, giving rise to a lot of water loss and hence having strong influence in the fields of hydrology, agronomy, ecology and civil engineering. Indeed, precisely predicting the evaporation rate from free water surface is of utmost importance, allowing the reasonable evaluation of water budget in irrigation management (Chartzoulakisa and Bertaki 2015), integrated lake basin management (Xiao *et al.* 2018, Zolá *et al.* 2019), and water resources development and management (Fowe *et al.* 2015, Zhao and Gao 2019). Furthermore, the water loss is also needed to be evaluated in the design of the air conditioning system in indoor swimming pools (Shah 2003, 2012, Asdrubali, 2009), the leakage evolution of nuclear spent-fuel disassembly basin (Pauken 1999), water change analysis in geotechnical engineering (Wang *et al.* 2017, Song *et al.* 2018a) and also the construction of passive evaporative cooling system of building (Tang and Etzion 2004, Cuce and Riffat 2016), etc. Beyond that, the free water evaporation rate is also taken as the potential evaporation rate when determining the actual evaporation rate of water evaporation from unsaturated soil surface (Song *et al.* 2018b). Therefore, it is important to well understand and modelling the process of water evaporation from free water surface to the atmosphere.

The process of evaporation at water-atmosphere

interface depends on both atmosphere and water parameters, such as air temperature, air relative humidity, wind speed (or air velocity), vapor pressure, and water temperature (Asdrubali 2009), etc. Therefore, many efforts have been made to investigate the free water evaporation process using various experimental methods, allowing the relationship between evaporation rate and the related influence factors to be revealed. The evaporation pan is a popular method for determining the evaporation from lakes, reservoirs and other large scale water surface in field (Piri *et al.* 2009). The corresponding evaporation rate can be obtained due to the change of water level. Notably, the pan evaporation is commonly affected by factors such as the size, colour, depth, material, installation mode, structures and position, strongly influencing on the results (Fu *et al.* 2004, 2009). In addition to the method mentioned above, the free water evaporation process can also be modelled and investigated in laboratory through wind tunnel (or climatic chamber), providing exactly controlled atmosphere conditions to water evaporation. By combing the wind tunnel and the large evaporation pan (standard class A pan), Pauken (1999) investigated the evaporation process of heated water (25°C-50°C) under free and forced convection conditions. The evaporation rate was indirectly determined through the mass change of a smaller pan which connected with the large evaporation pan. The results show that the evaporation rate increases nonlinearly with the vapor pressure deficit at lower wind speed. Furthermore, Jodat *et al.* (2012) conducted a similar evaporation experiment in a wind tunnel with a heated water pool, allowing the validity of Dalton based models and the similarity theory to be evaluated. Similarly, 28 evaporation tests under different conditions (e.g., water temperature between 27.6°C and 46.6°C, mean wind speed ranging from 0.101 m/s to 0.697 m/s) were performed by Raimundo *et al.* (2014) using low velocity wind tunnel with a evaporation tank equipped with heating system, revealing that wind speed has stronger influence on evaporation rate than other atmosphere

*Corresponding author, Ph.D.

E-mail: weikangsong@zzu.edu.cn

^aM.E.

E-mail: zhengdayibo@zzu.edu.cn

parameters. Recently, Blázquez *et al.* (2018) simulated the common operation conditions of indoor swimming pool using self-designed wind tunnel under different air flow conditions, validating the computational fluid dynamics based method for estimating free water evaporation. Similar to wind tunnel, the climatic chamber can also build fixed atmosphere condition between water and air. Thus, Asdrubali (2009) carried out an evaporation experiment using a small climatic chamber with an inserted water container. The results show that the evaporation rate increases with the increasing water temperature and decreasing relative humidity. Generally, based on the above analysis, most of the evaporation rate is determined by measuring the mass loss of water tank (or pan) in laboratory. Therefore, the measurement range of balance may limit the scale and accuracy of the model test to some degree. As an alternative, other climatic chambers which the evaporation rate can be obtained through the change of absolute relative humidity at the inlet and outlet of the chamber and the air flow rate has also been widely used (Mohamed *et al.* 2000, Song *et al.* 2013, 2018).

Various models have also been proposed for describing the free water evaporation process and predicting the related evaporation rate. The simplest model for predicting evaporation rate from water surface is multiplying a coefficient by pan evaporation results (Yihdego and Webb 2018), thus the determination of this coefficient becomes a challenge. The water budget model (e.g., Morton 1967, Zolá *et al.* 2019) is a common method to describe the water change in large scale water surface (e.g., lake, reservoir) when knowing the parameters such as precipitation, seepage, inflow and outflow. However, the lack of the measurement of seepage or inflow could restrict the application of this model (Singh and Xu 1997, Zolá *et al.* 2019). Considering the energy conservation of water body, the energy budget model (Winter *et al.* 2003, Lenters *et al.* 2005, Gianniou and Antonopoulos 2007) was also proposed for predicting water evaporation with parameters such as net radiation, the change in the energy content of the water body, sensible heat, etc. This type of model has been widely used in the lake evaporation evaluation (Blanken *et al.* 2011), but the availability of water temperature usually limits its application. In addition to the above models, the mass transfer model which based on Dalton's law has commonly applied to predicting the evaporation from the water surface as large as lake (Singh and Xu 1997, Zolá *et al.* 2019) or as small as pool indoor or outdoor (Simith *et al.* 1993, Pauken 1999, Shah 2012). The mass transfer model exhibits the nature of evaporation initiation, that is, vapour pressure deficit occurs between evaporating surface and atmosphere and the vapor is the transported by air turbulence. Correspondingly, this type of model is usually formed by different combinations of wind speed function with different expressions, air and water temperature function, air relative humidity function and vapour pressure function (Singh and Xu 1997, Pauken 1999). In general, the mass transfer model has a simple form and only needs a few easily obtained parameters, allowing daily evaporation from free water to be predicted accurately.

In this study, a mass-transfer based model was proposed and verified on the basis of large scale free water evaporation experiments performed in an environmental chamber. Firstly, the water evaporation process was

simulated in the chamber under controlled atmospheric conditions (i.e., increasing wind speed and air temperature). The atmospheric parameters (air temperature, relative humidity, wind speed, etc.) and the water temperature were monitored by various sensors for 7 days. Then, the existing popular models belonging to the mass transfer model were analyzed and evaluated using the experimental data. Finally, a new model was also proposed and verified on the basis of the obtained results. The new model helps better understand the mechanisms of water evaporation from free water surface, and can also be used for further calculation of potential evaporation rate.

2. Free water evaporation experiment

2.1 Experimental set-up

The free water evaporation test was conducted in a specially designed environmental chamber system (Fig. 1). The environmental chamber system is a large acrylic transparent chamber equipped with various sensors for measuring or monitoring both the atmospheric and water parameters (Song *et al.* 2013, 2016). Upon evaporation test, the compressed air flow from the air conditioning system was controlled by the flow regulator and then heated by a heating tube, supplying hot air to the chamber and forming various atmospheric conditions. Subsequently, the hot air was blown into the chamber and its relative humidity and temperature were also measured simultaneously. After passing through the chamber, the relative humidity and temperature of moist air were measured again before being

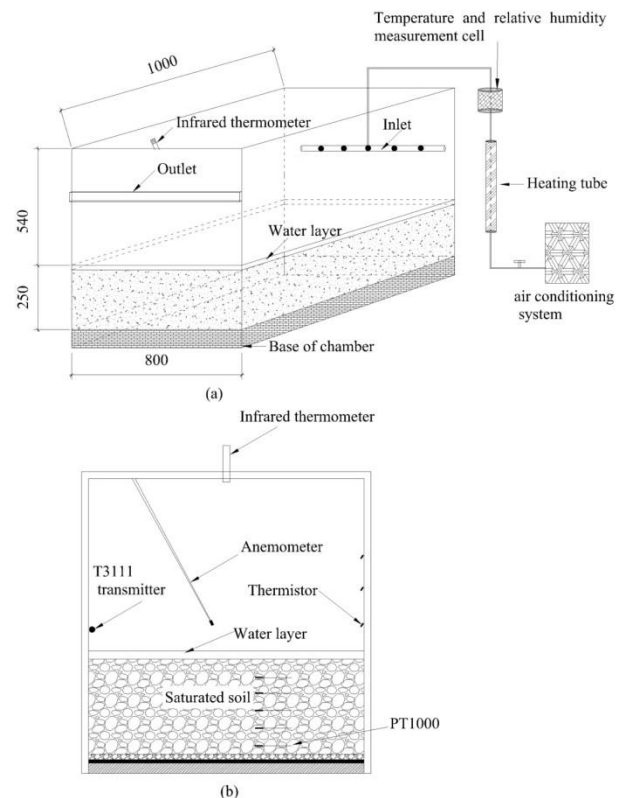


Fig. 1 Sketch of experimental set-up: (a) the environmental chamber system (dimensions: mm) and (b) sensors arrangements

discharged into the atmosphere. Note that the air flow rate was also monitored during evaporation test. The details of this environmental chamber can be seen in the work of Song *et al.* (2013).

The atmospheric parameters and water response during evaporation process are very important to understand the evaporation mechanism at water-atmosphere interface. Thus, a lot of sensors were installed at various positions of the chamber. In particular, three thermistors were fixed at different elevations along the chamber wall for monitoring air temperature (i.e., 50, 170, and 235 mm above the water surface). Three T3111 transmitters were used for monitoring the air relative humidity, one of them were installed at 50-mm height above water surface, the other two were used to measure the air relative humidity before and after passing through the chamber. Five temperature sensors (PT1000) were installed in the soil sample over depths (i.e., 50, 100, 150, 200, and 250 mm depths). Note that, this type of sensor was used for the further soil water evaporation test. An infrared thermometer (Pyropen-D) was also fixed at the end of chamber cover for measuring the water surface temperature. Besides of the sensors mentioned above, an anemometer (Testo 435-2) was used to measure the wind speed 50 mm above water surface inside the chamber. Notably, a ruler marked with scales was also pasted on the chamber wall for recording the change of water level inside the chamber.

2.2 Test procedure

According to the test plan, free water evaporation test was conducted before the soil water evaporation in this environmental chamber. Therefore, soil layer with a height of 250 mm was firstly compacted layer by layer, and various sensors for measuring both atmospheric parameter and water or soil temperature were installed at the pre-set positions during compaction. Then, a saturation process was performed using distilled water and finally a water layer with a thickness of 30 mm was formed on the soil surface.

After soil saturation, the free water evaporation test was conducted under different conditions: firstly, the heating tube temperature was kept the same (50°C) but the air flow rates were different: 60 L/min for the first day (Stage 1), 107 L/min for the next 1.7 days (Stage 2), and 158 L/min from $t = 2.7$ days to $t = 3.7$ days (Stage 3); secondly, the free water layer was evaporated at a constant air flow rate of about 158 L/min but different temperatures in heating tube: 100°C from $t = 3.7$ days to 4.7 days (Stage 4), 150°C from 4.7 days to 5.7 days (Stage 5) and 200°C from $t = 5.7$ days to the end of test (Stage 6).

The determination of evaporation rate using environmental chamber is based on the air absolute humidity difference between the inlet and outlet of the chamber and the corresponding air flow rate and the evaporating surface area (Mohamed *et al.* 2000):

$$E_a = 86400Q(h_{abs_out} - h_{abs_in})/\rho_w A \quad (1)$$

where E_a is the actual evaporation rate (mm/day), Q is the air flow rate (L/s), h_{abs_out} and h_{abs_in} are the air absolute humidity at outlet and inlet of the chamber (Mg/m³), respectively, ρ_w is the water density (Mg/m³), and A is the

surface area of water in the chamber (m²).

For the absolute relative humidity (h_{abs}), it can be calculated by Eq. (2) (Brutsaert 1988):

$$h_{abs} = 0.622e_a/(1000RT_{air}) \quad (2)$$

where R is the gas constant (287.04 J/(kg·K)), T_{air} is the air temperature (K), e_a is the air vapor pressure (Pa), and can be determined with the saturated vapor pressure and relative humidity, as follows:

$$e_a = e_s h_r / 100 \quad (3)$$

where e_s is the saturated vapor pressure (Pa) and h_r is the air relative humidity (%). The saturated vapor pressure is usually calculated using Eqs. (4) and (5) (Brutsaert 1988).

$$e_s = 101325 \exp \left(\frac{13.3185T_R - 1.976T_R^2}{-0.6445T_R^3 - 0.1299T_R^4} \right) \quad (4)$$

$$T_R = 1 - 373.15/T_{air} \quad (5)$$

3. General models for predicting free water evaporation

The mass transfer model is normally used to describing water evaporation process due to its simple form and clear physical meanings. As we know, the wind speed, vapor pressure and temperature were the major factors affecting the prediction results of the mass transfer model. Therefore, by introducing the wind speed function $f(u)$, the vapor pressure function $k(e)$ and temperature function $l(T)$ into Dalton equation, a generalized form of mass transfer model can be described as follows (Singh and Xu 1997):

$$E = f(u)k(e)l(T) \quad (6)$$

Table 1 shows various general forms of mass transfer model summarized by Singh and Xu (1997) with different functions of $f(u)$, $k(e)$ and $l(T)$. In Table 1, E is the free water evaporation rate (mm/day); e_s is the saturated vapor pressure deduced by the water or soil surface temperature (Pa); e_a is the air vapor pressure (Pa); T_a is the air temperature (°C) at a reference height; T_s is the surface temperature (°C); h_a is the air relative humidity at the reference height (%); u is the wind speed at the reference level (m/s). It is noted that the reference height is 50 mm above the water surface in this study. The parameters e_s and e_a can be determined using Eqs. (3) and (4), respectively.

In this study, these general forms in Table 1 are selected for further evaluation based on the experimental data obtained, expecting to find a suitable free water evaporation rate calculation model. Note that the choice of these models is based on the fact that they allow determination of the evaporation rate in a short term on one hand, and they represent most of the popular models on the other hand. Furthermore, these models contain at least two atmospheric parameters such as temperature and wind speed.

For each model, the related coefficients (a , b , and c) can be determined using the data from the free water evaporation tests under different atmospheric conditions. This process is conducted as follows: when the undetermined coefficients are related to wind speed, they

Table 1 General forms of mass transfer models

Number	General forms
Model 1	$E = au (e_s - e_a)$
Model 2	$E = a(1 - \exp(-u))(e_s - e_a)$
Model 3	$E = a(1 + bu)(e_s - e_a)$
Model 4	$E = au(e_s - e_a)(1 - b(T_a - T_s))$
Model 5	$E = a(1 + bu)(e_s - e_a)(1 - c(T_a - T_s))$
Model 6	$E = a(T_a + 25)^2 (100 - h_a)$

will be determined using the data obtained from the evaporation test with different wind speeds (i.e., Stage 1 to Stage 3); when the undetermined coefficients are related to temperature, they will be determined using the data obtained from the evaporation test with different heating temperatures (i.e., Stage 4 to Stage 6). After the determination of parameters, the models are also needed to be verified by experimental data. According to the ways for the parameters determination, the verification of the models is conducted in two different fashions: when the coefficients in the model are determined using the data obtained with different wind speeds, the models will be verified based on the data obtained with different temperatures; reversed process will be followed in the second case. Finally, the prediction results are compared with the experimental results to verify the relevance of the models. The model with a good performance will be selected as the free water evaporation model in this study.

4. Results of experiment and model evaluation

4.1 Experimental results

The evolutions of air flow rate are shown in Fig. 2. As shown in this figure, the air flow rate fluctuates around 60 L/min in the first day, and then reaches 107 L/min and stays at this value until $t = 2.7$ days. Later, it increases up to a value as high as 158 L/min. After $t = 4.7$ days, it shows a slight decrease and stabilizes at values of 155 L/min, 150 L/min and 147 L/min in Stage 4, Stage 5 and Stage 6, respectively. Furthermore, three different wind speeds at 50-mm height corresponding to these air flow rates can be identified: 0.14 m/s in Stage 1, 0.26 m/s in Stage 2 and 0.44 m/s in other stages.

The changes of air temperatures at the inlet, outlet of chamber are shown in Fig. 3. In general, the air temperatures decreases along with the increasing air flow rate during the first 3.7 days and then it increases following the increasing temperature in the heating tube until the end of test. The air temperature at inlet is much higher than that at outlet. It decreases at a low rate from 25°C to 18.7°C from Stage 1 to Stage 3. After that, it sharply increases to the first stabilization at a value of 34°C (Stage 4), and then to the second one at a value of 48.2°C (Stage 5). Finally, it

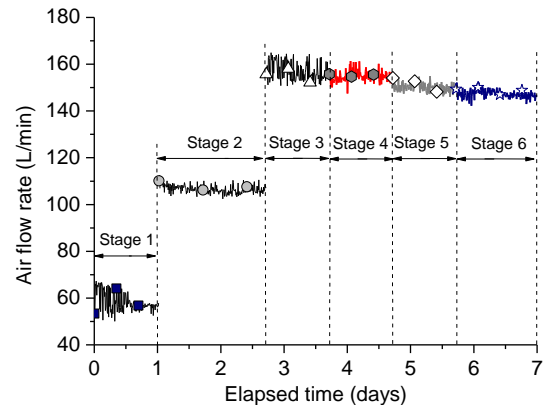


Fig. 2 Evolutions of air flow rate

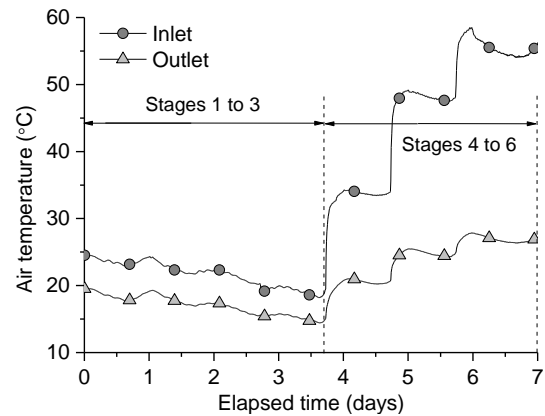


Fig. 3 Evolutions of air temperature at the inlet and outlet of chamber

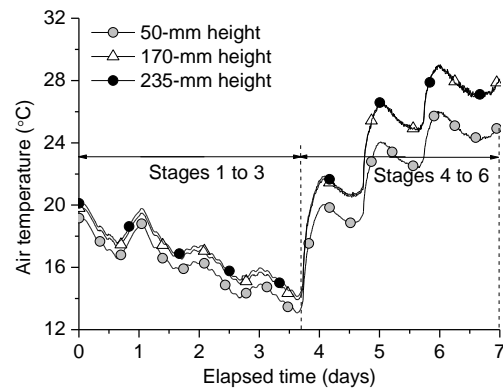


Fig. 4 Evolutions of air temperature at different elevations

reaches the third constant stage at the highest value of 55.5°C (Stage 6). As far as the temperature in the outlet is concerned, the value decreases from 20.7°C to 14.5°C in the first three stages. Afterwards, the value starts to increase with three stabilization stages at 20.5°C, 24.7°C and 27°C, respectively. The large temperature gap between inlet and outlet of the chamber indicates an energy consumption process happened in the chamber, that is, the water evaporation process.

Fig. 4 shows changes in air temperature in the chamber over time for different elevations. The values increase and decrease in the first three stages and then increase with three constant stages following the air temperature at the

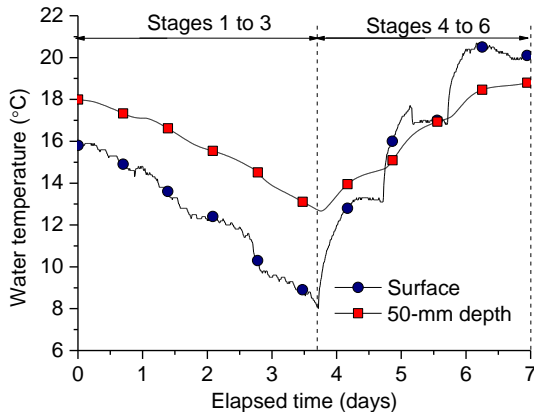


Fig. 5 Evolutions of water temperatures at different positions

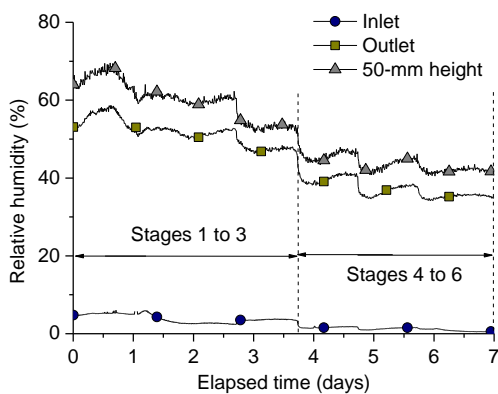


Fig. 6 Evolutions of air relative humidity at different locations in the chamber

inlet of chamber: the temperature values at different heights in the chamber varies from 20.8°C to 13°C in the first 3.7 days and the values at the 170 and 235-mm heights are higher than that at the 50-mm heights. During Stages 4 to 6, following the increase of heating tube temperature, three temperature plateaux can be observed at different locations. Furthermore, the values are quite similar in the zone above the 50-mm height and higher than that at the 50-mm height.

The evolutions of water temperature at different depths are shown in Fig. 5. In general, a two-stage evolution can be identified: a gradual decrease over time in the first 3.7 days followed by an increase until the end of test. The temperature at the water surface shows the lowest value during the first 3.7 days while the trend is inversed in the left of time. Indeed, the value decreases from 16°C to 8°C in the first 3.7 days. After that, it increases and reaches some almost stable stages. This result confirms an energy exchange process during water evaporation: the energy for evaporation is mainly from water body in the first 3.7 days (temperature decrease), and then the hot air supplies most of the energy for evaporation and heats the water in the meantime (temperature increase). Note that the temperature at 50-mm depth shows the similar evolution trend.

The changes of air relative humidity are shown in Fig. 6. In general, the imposed relative humidity at inlet is extremely low, i.e., less than 5%. The values in the chamber are much higher than that at inlet and decreases regularly with different plateaux. The relative humidity at

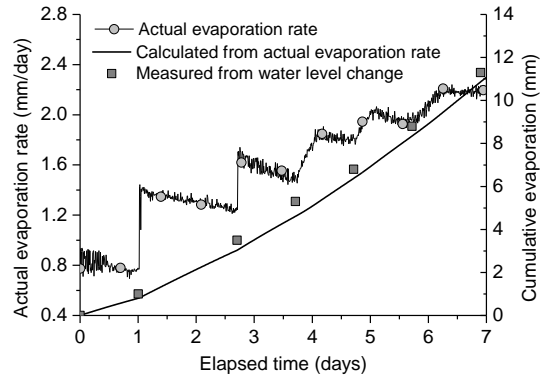


Fig. 7 Evolutions of actual evaporation rate and cumulative evaporation

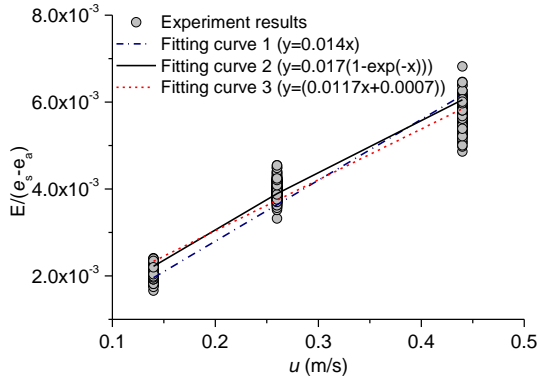
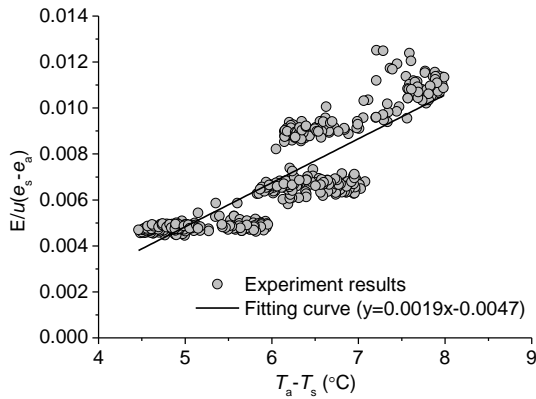
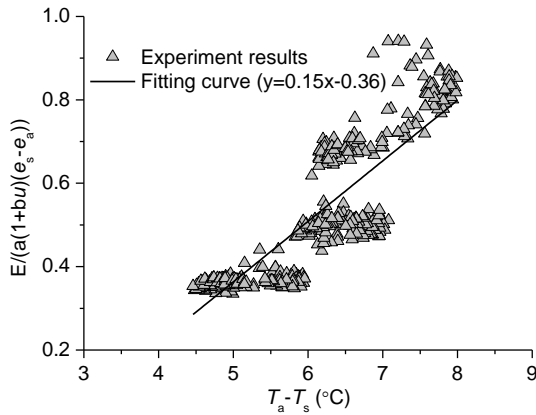
the 50-mm height exhibits the highest value and the one at inlet is the lowest. The effects of air temperature and air flow rate on the relative humidity inside the chamber are visible. For instance, at 50-mm height, when the air flow rate increases in three steps, a decrease of relative humidity can be identified, with three plateaux at 68.5%, 60% and 53.5% relative humidity, respectively. Similarly, when the temperature in the heating tube increases in three steps, a decrease of relative humidity can also be identified, with three plateaux at 46%, 43%, and 41% relative humidity, respectively.

The actual evaporation rate determined following Eq. (1) is plotted in Fig. 7. Six plateaux can be identified: during the first stage with imposed air flow rate, the value reaches the first stabilization. The subsequent increases of air flow rate gives rise to growth of the actual evaporation rate. Thereby, the three plateaux are at 0.8, 1.32, and 1.57 mm/day, corresponding to the three imposed air flow rates, respectively. For the temperature imposing stages (Stages 4, 5 and 6), the actual evaporation rate is increasing with the increase of imposed temperature and three plateaux are observed at 1.79, 1.97, and 2.15 mm/day, respectively. For the cumulative evaporation, two methods are applied to the calculation: calculating from the actual evaporation rate and directly measuring from the water level change. A very good agreement is obtained between the measured and calculated values, indicating the reliability of the evaporation measurement using this chamber.

4.2 Parameters determination

The data from the free water evaporation test with different wind speeds (Stages 1 to 3) are used to determine coefficients a in Models 1 to 3 and b in Model 3. For this purpose, the ratio of evaporation rate (E) to the vapor pressure deficit ($e_s - e_a$) with three different wind speeds is calculated and considered as the value of au , $a(1 - \exp(-u))$ and $a(1 + bu)$, respectively. Then, the relationship between $E/(e_s - e_a)$ and u can be observed in Fig. 8. Therefore, the coefficient a can be determined: $a = 0.014$ (Model 1), 0.017 (Model 2) and 0.0007 (Model 3). Similarly, the coefficient b in Model 3 can also be determined: $b = 16.72$.

For the Model 4, the value of $E/u(e_s - e_a)$ can be calculated by the experimental data from the evaporation tests with different heating temperatures (Stages 4 to 6).

Fig. 8 Relationship between $E/(e_s - e_a)$ and u Fig. 9 Relationship between $E/u(e_s - e_a)$ and $T_a - T_s$ Fig. 10 Relationship between $E/(a(1+bu)(e_s - e_a))$ and $T_a - T_s$

Therefore, a linear relationship between $E/u(e_s - e_a)$ and $T_a - T_s$ can be observed in Fig. 9, giving $a = -0.0047$ and $b = 0.404$.

For the Model 5, three coefficients (a , b and c) are needed to be determined. The Model 5 can be considered as the combination of the Model 3 and $1 - c(T_a - T_s)$. Therefore, by letting coefficients a and b equal to the values determined in Model 3, the relationship between $E/(a(1+bu)(e_s - e_a))$ and $T_a - T_s$ can be obtained using the data from free water evaporation under different heating temperature (Stages 4 to 6) (see Fig. 10). However, the linear relationship in this figure is in conflict with the expression $1 - c(T_a - T_s)$. To tackle this problem, expression $1 - c(T_a - T_s)$ is replaced by $d + c(T_a - T_s)$ for describing the temperature influence. Thereby, Model 7 is obtained:

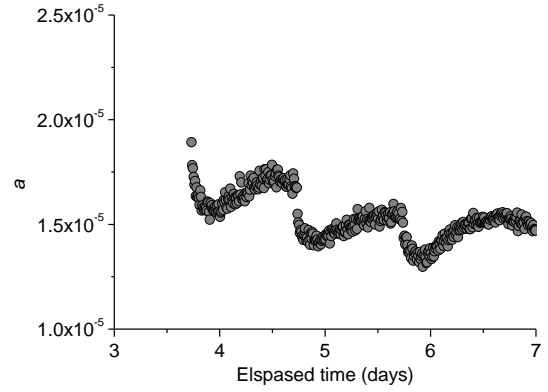
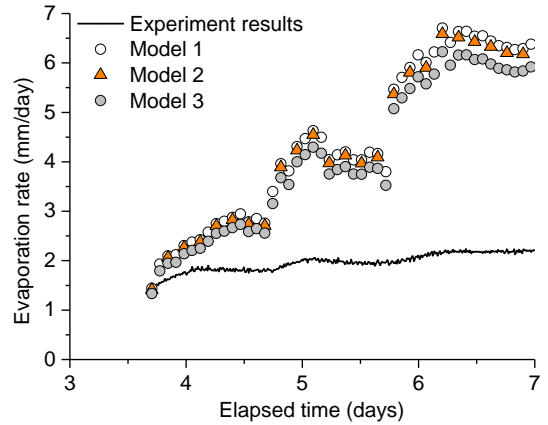
Fig. 11 Determination of coefficient a 

Fig. 12 Verification of Models 1 to 3 (Stages 4 to 6)

$$E = a(1 + bu)(e_s - e_a)[d + c(T_a - T_s)] \quad (7)$$

Using the relationship between $T_a - T_s$ and $E/(a(1+bu)(e_s - e_a))$ shown in Fig. 10, coefficients c and d can be determined: $c = 0.15$; $d = -0.36$.

For the Model 6, only one coefficient a is involved and can be determined using the measured evaporation test data at constant wind speed with different air temperatures (Stages 4 to 6) (Fig. 11). As can be observed in Fig. 11, the value of a fluctuates with changes of air temperature. An average value of 1.53×10^{-5} can be obtained.

4.3 Model evaluation

The Models 1 to 3 are firstly verified using the results from the evaporation experiment with different heating tube temperatures (Stages 4 to 6). As can be seen in Fig. 12, the predicted and measured evaporation rates show the same evolution trend: the evaporation rate increases with increasing air temperature in the chamber. Different plateaus in Fig. 12 correspond to different atmospheric conditions. However, the predicted values are much higher than the measured ones. This indicates that if Models 1 to 3 are calibrated with wind speed, it cannot predict the evaporation correctly in case of variable temperatures.

Fig. 13 shows the experimental data and the prediction of Models 4, 6 and 7. As shown in Fig. 13, there is significant deviation between the measured and predicted results, especially in Models 4 and 7. Therefore, even with a

temperature related parameter, Models 4, 6 and 7 are not able to predict the free water evaporation rate satisfactorily.

5. Development and verification of new model

According to the verification of different models using experimental data, the general mass transfer based models are inefficient in predicting free water evaporation. However, the models with linear wind function (Models 1 to 3) or with relative humidity function (Model 6) can give acceptable prediction results under the condition of increasing wind speed or air temperature, respectively (Figs. 14 and 15). Therefore, a new model (Model 8) contains wind function and air relative humidity function is proposed in this study, as follows:

$$E = (a + bu)(100 - h_a) \tag{8}$$

In Model 8, only two easily available parameters, i.e., wind speed and air relative humidity are introduced, and two undetermined coefficients related to wind speed (*a* and *b*) are needed to be determined. For determining these coefficients, the data obtained from the water evaporation test with different wind speeds (Stages 1 to 3) are used to generate the linear relationship between $E/(100-h_a)$ and *u* (see Fig. 16), giving $a = 0.022$ and $b = 0.031$.

After determining the coefficients, Model 8 was verified

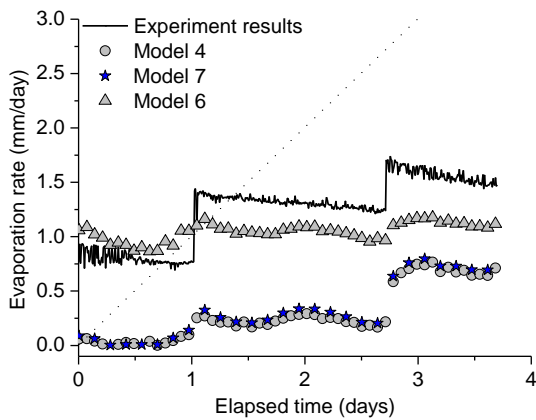


Fig. 13 Verification of Models 4, 6 and 7 (Stages 1 to 3)

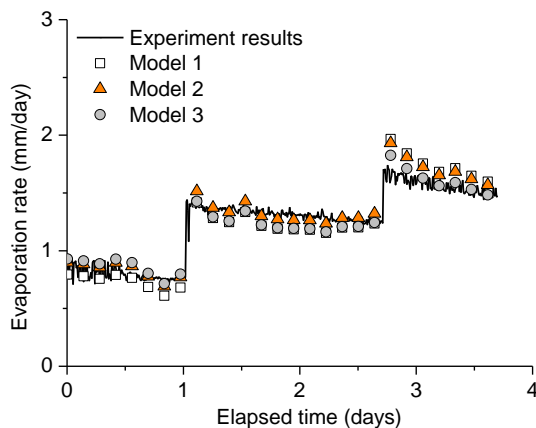


Fig. 14 Comparison between model prediction (Models 1 to 3) and experimental measurements (Stages 1 to 3)

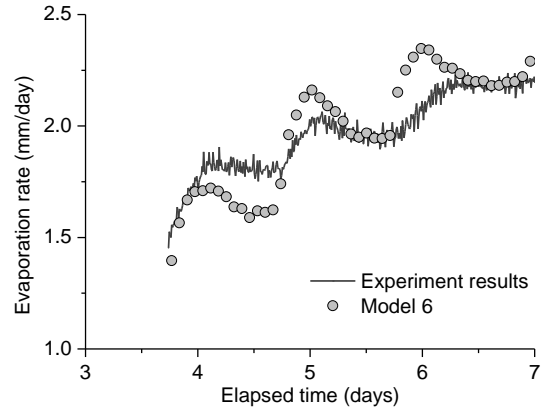


Fig. 15 Comparison between model predictions (Model 6) and experimental measurements (Stages 4 to 6)

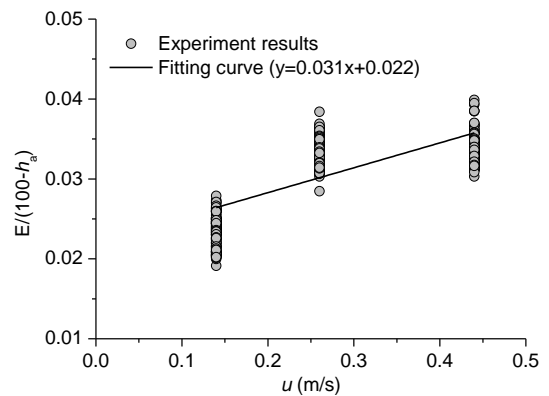


Fig. 16 Relationship between $E/(100-h_a)$ and *u*

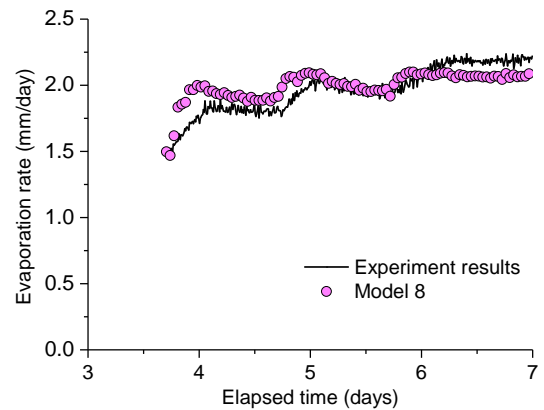


Fig. 17 Verification of Model 8

using the experimental results obtained from the water evaporation test with increasing heating temperature (Stages 4 to 6). The measured and calculated evaporation rates are shown in Fig. 17. As can be seen in this figure, both the predicted and measured values are increasing with the increasing heating temperature (Stages 4 to 6). The predicted values agree well with the measured ones. In conclusion, Model 8 is reliable to predict the free water evaporation rate with varying atmospheric conditions.

6. Conclusions

In order to modelling the free water evaporation process, a large scale evaporation test was firstly conducted in an

environmental chamber and then various models reported in the literature were assessed based on the experimental data. Finally, a new model was proposed and verified using the related experimental data. More specific conclusions are drawn as follows:

- The free water evaporation is mainly affected by the atmospheric parameters. The evaporation rate increases with the increasing air temperature and wind speed.
- The relative humidity inside the chamber decreases with the increases of air flow rate and heating tube temperature.
- Both the air and water temperatures are affected by the energy transfer during evaporation. When water evaporation is processed at increasing air flow rate, the evaporation process consumes energy from air and water layer. Hence, the temperatures of air and water surface decrease with the increasing evaporation rate. On the contrary, when water evaporation is processed at increasing heating temperature, part of the energy from hot air will contribute to heat air and water layer. Therefore, their temperatures increase along with the increase of evaporation rate.
- Model 8 is the most relevant one for predicting free water evaporation under different atmospheric conditions.

Acknowledgments

The research described in this paper was financially supported by the Key Scientific Research Project of the Higher Education Institutions of Henan Province (Grant No. 18A560024), the National Key R&D Program of China (Grant No. 2017YFC1502600), and the China Postdoctoral Science Foundation funded project (Grant No. 2018T110742, 2016M592312).

References

- Asdrubali, F. (2009), "A scale model to evaluate water evaporation from indoor swimming pools", *Energy Build.*, **41**(3), 311-319. <https://doi.org/10.1016/j.enbuild.2008.10.001>.
- Blanken, P.D., Spence, C., Hedstrom, N. and Lenters, J.D. (2011), "Evaporation from Lake Superior: 1. Physical controls and processes", *J. Great Lakes Res.*, **37**(4), 707-716. <https://doi.org/10.1016/j.jglr.2011.08.009>.
- Blázquez, J.L.F., Maestre, I.R., Gallero, F.J.G. and Gómez, P.Á. (2018), "Experimental test for the estimation of the evaporation rate in indoor swimming pools: Validation of a new CFD-based simulation methodology", *Build. Environ.*, **138**, 293-299. <https://doi.org/10.1016/j.buildenv.2018.05.008>.
- Brutsaert, W. (1988), *Evaporation into the Atmosphere: Theory, History, and Applications*, D. Reidel Publishing Company, Dordrecht, The Netherlands.
- Chartzoulakisa, K. and Bertaki, M. (2015), "Sustainable water management in agriculture under climate change", *Agric. Agric. Sci. Procedia*, **4**, 88-98. <https://doi.org/10.1016/j.aaspro.2015.03.011>.
- Cuce, P.M. and Riffat, S. (2016), "A state of the art review of evaporative cooling systems for building applications", *Renew. Sust. Energy Rev.*, **54**, 1240-1249. <https://doi.org/10.1016/j.rser.2015.10.066>.
- Fowe, T., Karambiri, H., Paturel, J.E., Poussin, J.C. and Cecchi, P. (2015), "Water balance of small reservoirs in the Volta basin: A case study of Boura reservoir in Burkina Faso", *Agric. Water Manage.*, **152**, 99-109. <https://doi.org/10.1016/j.agwat.2015.01.006>.
- Fu, G.B., Charles, S.P. and Yu, J.J. (2009), "A critical overview of pan evaporation trends over the last 50 years", *Clim. Change*, **97**(1-2), 193-214. <https://doi.org/10.1007/s10584-009-9579-1>.
- Fu, G.B., Liu, C.M., Chen, S.L. and Hong, J.L. (2004), "Investigating the conversion coefficients for free water surface evaporation of different evaporation pans", *Hydrol. Process.*, **18**(12), 2247-2262. <https://doi.org/10.1002/hyp.5526>.
- Gianniou, S.K. and Antonopoulos, V.Z. (2007), "Evaporation and energy budget in Lake Vegoritis, Greece", *J. Hydrol.*, **345**(3-4), 212-223. <https://doi.org/10.1016/j.jhydrol.2007.08.007>.
- Jodat, A., Moghiman, M. and Anbarsooz, M. (2012), "Experimental comparison of the ability of Dalton based and similarity theory correlations to predict water evaporation rate indifferent convection regimes", *Heat Mass Transfer*, **48**(8), 1397-1406. <https://doi.org/10.1007/s00231-012-0984-z>.
- Lenters, J., Kratz, T. and Bowser, C. (2005), "Effects of climate variability on lake evaporation: results from a long-term energy budget study of Sparkling Lake, northern Wisconsin (USA)", *J. Hydrol.*, **308**, 168-195. <https://doi.org/10.1016/j.jhydrol.2004.10.028>.
- Mohamed, A.A., Sasaki, T. and Watanabe, K. (2000), "Solute transport through unsaturated soil due to evaporation", *J. Environ. Eng.*, **126**(9), 842-848. [https://doi.org/10.1061/\(ASCE\)0733-9372\(2000\)126:9\(842\)](https://doi.org/10.1061/(ASCE)0733-9372(2000)126:9(842)).
- Morton, F. (1967), "Evaporation from large deep lakes", *Water Resour. Res.*, **3**(1), 181-200. <https://doi.org/10.1029/WR003i001p00181>.
- Pauken, M.T. (1999), "An experimental investigation of combined turbulent free and forced evaporation", *Exp. Therm. Fluid Sci.*, **18**(4), 334-340. [https://doi.org/10.1016/S0894-1777\(98\)10038-9](https://doi.org/10.1016/S0894-1777(98)10038-9).
- Piri1, J., Amin, S., Moghaddamia, A., Keshavarz, A., Han, D. and Remesan, R. (2009), "Daily pan evaporation modeling in a hot and dry climate", *J. Hydrol. Eng.*, **14**(8), 803-811. [https://doi.org/10.1061/\(ASCE\)HE.1943-5584.0000056](https://doi.org/10.1061/(ASCE)HE.1943-5584.0000056).
- Raimundo, A.M., Gaspar, A.R., Oliveira, A.V.M. and Quintela, D.A. (2014), "Wind tunnel measurements and numerical simulations of water evaporation in forced convection airflow", *Int. J. Therm. Sci.*, **86**, 28-40. <https://doi.org/10.1016/j.ijthermalsci.2014.06.026>.
- Shah, M.M. (2003), "Prediction of evaporation from occupied indoor swimming pools", *Energy Build.*, **35**(7), 707-713. [https://doi.org/10.1016/S0378-7788\(02\)00211-6](https://doi.org/10.1016/S0378-7788(02)00211-6).
- Shah, M.M. (2012), "Improved method for calculating evaporation from indoor water pools", *Energy Build.*, **49**, 306-309. <https://doi.org/10.1016/j.enbuild.2012.02.026>.
- Singh, V.P. and Xu, C.Y. (1997), "Evaluation and generalization of 13 mass-transfer equations for determining free water evaporation", *Hydrol. Process.*, **11**(3), 311-323. [https://doi.org/10.1002/\(SICI\)1099-1085\(19970315\)11:3<311::AID-HYP446>3.0.CO;2-Y](https://doi.org/10.1002/(SICI)1099-1085(19970315)11:3<311::AID-HYP446>3.0.CO;2-Y).
- Song, L., Li, J., Garg, A. and Mei, G. (2018a), "Experimental study on water exchange between crack and clay matrix", *Geomech. Eng.*, **14**(3), 283-291. <https://doi.org/10.12989/gae.2018.14.3.283>.
- Song, W.K., Cui, Y.J. and Ye, W.M. (2018b), "Modelling of water evaporation from bare sand", *Eng. Geol.*, **233**, 281-289. <https://doi.org/10.1016/j.enggeo.2017.12.017>.
- Song, W.K., Cui, Y.J., Tang, A.M. and Ding, W.Q. (2013), "Development of a large scale environmental chamber for investigating soil water evaporation", *Geotech. Test. J.*, **36**(6),

- 847-857. <https://doi.org/10.1520/GTJ20120142>.
- Song, W.K., Cui, Y.J., Tang, A.M., Ding, W.Q. and Wang, Q. (2016), "Experimental study on water evaporation from compacted clay using environmental chamber", *Can. Geotech. J.*, **53** (8), 1293-1304. <https://doi.org/10.1139/cgj-2015-0415>.
- Tang, R. and Etzion, Y. (2004), "Comparative studies on the water evaporation rate from a wetted surface and that from a free water surface", *Build. Environ.*, **39**(1), 77-86. <https://doi.org/10.1016/j.buildenv.2003.07.007>.
- Wang, Z., Kwon, S., Qiao, L., Bi, L. and Yu, L. (2017), "Estimation of groundwater inflow into an underground oil storage facility in granite", *Geomech. Eng.*, **12**(6), 1003-1020. <https://doi.org/10.12989/gae.2017.12.6.1003>.
- Winter, T., Buso, D., Rosenberry, D., Likens, G., Sturrock Jr., A. and Mau, D. (2003), "Evaporation determined by the energy-budget method for Mirror Lake, New Hampshire", *Limnol. Oceanogr.*, **48**(3), 995-1009. <https://doi.org/10.4319/lo.2003.48.3.0995>.
- Xiao, K., Griffisa, T.J., Bakera, J.M., Bolstad, P.V., Erickson, M.D., Leed, X., Wood, J.D., Hu, C. and Nieber, J.L. (2018), "Evaporation from a temperate closed-basin lake and its impact on present, past, and future water level", *J. Hydrol.*, **561**, 59-75. <https://doi.org/10.1016/j.jhydrol.2018.03.059>.
- Yihdego, Y. and Webb, J.A. (2018), "Comparison of evaporation rate on open water bodies: Energy balance estimate versus measured pan", *J. Water Clim. Change*, **9**(1), 101-111. <https://doi.org/10.2166/wcc.2017.139>.
- Zhao, G. and Gao, H. (2019), "Estimating reservoir evaporation losses for the United States: Fusing remote sensing and modeling approaches", *Remote Sens. Environ.*, **226**, 109-124. <https://doi.org/10.1016/j.rse.2019.03.015>.
- Zolá, R.P., Bengtsson, L., Berndtsson, R., Martí-Cardona, B., Satgé, F., Timouk, F., Bonnet, M.P., Mollericon, L., Gamarra, C. and Pasapera, J. (2019), "Modelling Lake Titicaca's daily and monthly evaporation", *Hydrol. Earth Syst. Sci.*, **23**(2), 657-668. <https://doi.org/10.5194/hess-23-657-2019>.